

1
2
3
4
5
6
7
8
9
10
11
12
13
14
15
16
17
18
19
20
21
22
23
24
25
26
27
28
29
30
31
32
33
34
35
36
37
38
39

submitted to Geophys. Res. Lett.

U.S. weather extremes and El Niño

Gerald A. Meehl^{a*}, Claudia Tebaldi^a,
Haiyan Teng^a and Thomas C. Peterson^b

a) National Center for Atmospheric Research (1)
PO Box 3000
Boulder CO 80307

b) NOAA's National Climatic Data Center
151 Patton Avenue
Asheville, NC 28801

June 15, 2007

* Corresponding author: meehl@ncar.ucar.edu 303-497-1331

(1) The National Center for Atmospheric Research is sponsored by the National Science Foundation

40 **Abstract**

41 A global coupled climate model representative of the current generation of models is
42 shown to simulate most first order aspects of El Niño events, their teleconnections over
43 North America, and the associated observed patterns of extremes in present-day climate.
44 Future El Niño teleconnection patterns over the U.S. are projected to shift eastward and
45 northward due in part to the different midlatitude base state atmospheric circulation in a
46 warmer climate. Consequently, projections for the changes in the patterns of extremes
47 over the U.S. during future El Niño events include: decreases of frost days over the
48 southwestern U.S expand northward and eastward; increases in intense precipitation in
49 the SW U.S. expands eastward and areas in the SE U.S. become stronger; and decreases
50 of heat wave intensity over much of the southern tier of states turn to increases.

51

52

53 **1. Introduction**

54 Weather and climate extremes could have some of the most serious consequences for
55 human society, wildlife and ecosystems in a future warmer climate (Easterling et al.,
56 2000; Meehl et al., 2000). Thus, there has been considerable work done looking at
57 possible mean changes of extremes in a future warmer climate (e.g. see assessment in
58 Meehl et al., 2007a). However, patterns of extremes are affected by modes of circulation
59 such as El Niño (Gershunov and Barnett, 1998; Cayan et al., 1999; Schubert et al.,
60 2005). Temperature and precipitation extremes, with their serious impacts, have been
61 shown to play a major role in exacerbating the disruptive effects associated with El Niño
62 events over the U.S. (Glantz, 2001). Changes of future extremes have been linked to

63 modes of circulation like the North Atlantic Oscillation (e.g. Scaife et al., 2007), but no
64 study has yet addressed the possible future patterns of extremes associated with El Niño
65 events over the U.S.

66

67 It has been demonstrated that the current generation of climate models is improved
68 compared to previous versions, and they now are able to simulate most first order aspects
69 of El Niño events in present-day climate (e.g., Meehl and Teng, 2007). Therefore, the
70 purpose of this paper is to examine El Niño teleconnections over the U.S. in terms of
71 extremes for present-day climate, review how those teleconnections could change in a
72 future warmer climate, and then show how those changes could influence the patterns of
73 extremes over the continental U.S. associated with future El Niño events.

74

75

76 **2. Models and observed data**

77

78 The WCRP CMIP3 multi-model dataset archived at PCMDI (Meehl et al., 2007b)
79 includes the Frich et al. (2002) extremes indices from a subset of models, and a global
80 analysis of future changes for a number of the extremes indices has been performed for
81 those models (Tebaldi et al., 2006). However, those model data do not include all the
82 data necessary to perform an analysis of the relationship of El Niño events to the
83 extremes indices for the relevant experiments. Therefore, here we focus on one model
84 (the Parallel Climate Model, PCM) that has been shown to simulate 20th century
85 extremes over the U.S. reasonably well in terms of frost days (Meehl et al., 2004a), heat

86 waves (Meehl and Tebaldi, 2004), and precipitation intensity (Meehl et al., 2005a). This
87 model has also been used to demonstrate that recent observed trends in temperature
88 extremes over the U.S. have mostly been due to anthropogenic forcings (Meehl et al.,
89 2007c).

90

91 The PCM is described, for example, by Meehl et al. (2004b), and its resolution of the
92 atmosphere is T42, or roughly $2.8^\circ \times 2.8^\circ$, with 18 levels in the vertical. Resolution in
93 the ocean is roughly $\frac{2}{3}$ degree tapering down to $\frac{1}{2}$ degree in the equatorial tropics, with
94 32 levels. No flux adjustments are used in the model, and, at least in terms of global-
95 mean temperature, a relatively stable climate is simulated.

96

97 The PCM was run for a pre-industrial (1870) control run which provided initial states for
98 the 20th century simulations. Four member ensembles of PCM 20th century climate
99 experiments were run with a combination of anthropogenic and natural forcings. These
100 20th century simulations were started from different times in the 1870 control run
101 separated by 10 to 20 years. The natural (volcanoes and solar) and anthropogenic
102 (greenhouse gases, sulfate aerosols, and ozone) forcings used in these experiments are
103 described in Meehl et al. (2004b).

104

105 The observed data are the extremes indices (Frich et al., 2002) derived from daily data,
106 updated and described by Alexander et al. (2006). A pre-computed set of seasonal and
107 annual indices, with global coverage, is available as the HadEX dataset
108 (<http://hadobs.metoffice.com/hadex/>) but for our purpose the indices need to be computed

109 over a year defined more congruous to the ENSO year (e.g. Meehl, 1987) spanning the
110 June-to-May period. Therefore, we computed the indices from observed daily data from
111 Canada, Mexico and the United States. These data and their quality control, homogeneity
112 assessments, and gridding methodology are described in Peterson et al. (2007). We also
113 added the heat wave intensity index of Karl and Knight (1997), described below. We
114 used sea level pressure fields from the NCEP/NCAR reanalyses to identify El Niño (La
115 Niña) events.

116

117 Frost days are defined as days when the temperature goes below freezing, and the
118 corresponding index counts the number of such days during the year. The heat wave
119 intensity index (Karl et al., 1997, and applied by Meehl and Tebaldi, 2004) has been
120 defined in light of the fact that during the Chicago heat wave of 1995, the worst effects
121 on excess human mortality were observed after three consecutive very hot nights.
122 Therefore, the heat wave intensity index is defined as the mean of the annual three
123 consecutive warmest nights. Precipitation intensity is defined as the total annual
124 precipitation amount divided by the number of wet days, but in our study we isolate
125 precipitation intensity over the winter season (DJF).

126

127 El Niño (La Niña) events are defined as the 1-5 year filtered Niño3.4 area-averaged sea
128 surface temperature anomaly that positively (negatively) exceeds one standard deviation
129 for the DJF season (e.g. Meehl and Teng, 2007). Accordingly, we label the June-May
130 year covering that season as an El Niño (La Niña) year and we stratify the geographical
131 patterns accordingly. For the PCM control run (200 years), there are 32 El Niño events,

132 and 35 La Niña events. For the 100 years of the stabilized A1B experiment (2100-2199,
133 concentrations increase from 2000 to 2099 according to the mid-range A1B scenario, and
134 then all concentrations are held fixed after 2100, see Meehl et al., 2005), there are 12 El
135 Niño events, and 16 La Niña events. For the 57 years covered by the NCEP/NCAR
136 reanalysis (1948-2004), there are 13 El Niño events and 11 La Niña events. The daily
137 data from which the extremes indices are computed covers 55 of the 57 years (1950-
138 2004) and the same 24 events. All differences are computed as El Niño minus La Niña.

139

140 3. El Niño teleconnections over North America, present and future

141

142 Figure 1 (top left) shows composite sea level pressure (SLP) anomaly patterns for DJF,
143 El Niño minus La Niña, for the model, and can be compared to a similar composite from
144 the NCAR/NCEP reanalyses (Fig. 1 middle left). The typical El Niño pattern is
145 represented in the observations, with an anomalously deepened Aleutian Low (center of
146 negative SLP anomalies in the North Pacific near the Aleutian Islands), a small
147 anomalous high over the Rockies (positive SLP anomalies) and stronger positive SLP
148 anomalies over northern Canada, and anomalous negative SLP anomalies over the
149 southeast U.S. and eastern seaboard extending out over the Atlantic. For the model, the
150 anomalous low center in the North Pacific is shifted somewhat south and east, with small
151 amplitude negative SLP anomalies extending across the U.S., but with positive SLP
152 anomalies over northern Canada as in the observations. The anomalous low SLP center
153 in the Atlantic is shifted eastward in the model compared to observations. The result,
154 portrayed as differences of anomalies, model minus observed (Fig. 1, bottom left). shows

155 the southward shifted anomalous Aleutian Low in the model as negative SLP differences
156 in the central North Pacific and positive SLP differences in the northern North Pacific,
157 with negative SLP differences over the Rockies, and positive SLP differences over the
158 Atlantic. The PCM is typical of other current models in this regard, as shown by Meehl
159 and Teng (2007) where they describe how the position of the various El Niño
160 teleconnection low and high centers are related to the location of the equatorial Pacific
161 sea surface temperature (SST) anomalies and corresponding precipitation and consequent
162 convective heating anomalies.

163

164 El Niño events in the future stabilized A1B experiment (Fig. 1 top right) show a different
165 teleconnection pattern compared to the control run in Fig. 1 (top left). The anomalous
166 Aleutian Low is shifted eastward and northward (as indicated by the differences in Fig. 1
167 middle right), with a reduction in the amplitude of the anomalous positive SLP anomalies
168 over northern Canada, and a deepening of the anomalous low pressure in the Atlantic.
169 This future change in the El Niño teleconnection pattern over North America is also
170 typical of other current models, and is associated in large part with the change in
171 midlatitude base state circulation due to the increase of anthropogenic greenhouse gases
172 (Meehl and Teng, 2007). Though changes in future El Niño amplitude can also play a
173 role, the stabilized A1B experiment in PCM shows virtually no change in future El Niño
174 amplitude (standard deviation of the 1-5-yr filtered Niño3.4 SST for observed events
175 from the NCEP/NCAR reanalyses is 0.77°C , for the PCM control run is 0.74°C , and the
176 PCM stabilized_A1B is 0.74°C). The PCM produces somewhat reduced amplitude El
177 Niño events for much greater forcing (e.g. 4XCO₂, Meehl et al., 2006). Thus, for the

178 experiments considered here, the major cause of the changes in future El Niño
179 teleconnections is the changed midlatitude base state.

180

181

182 **4. Present-day and future patterns of U.S. extremes during El Niño**

183 The observed pattern of present-day frost days during El Niño events is shown in Fig. 2a,
184 and is characterized by decreases in the northwest U.S. and Great Basin, and increases in
185 the southern and eastern U.S. The PCM representation of this pattern for present day El
186 Niño events is similar (Fig. 2b), with more consistent decreases in frost days extending
187 farther down the west coast in the model as a consequence of the southward-shifted
188 anomalous low pressure in the North Pacific (Fig. 1b). The overall pattern of frost days
189 during El Niño events in the model (Fig. 2b) is much smoother compared to the
190 observations (Fig. 2a) due in part to the longer period of the control run and the much
191 greater number of El Niño events in the model compared to the relatively fewer number
192 of events in the short observational record. As could be expected from the future
193 northward and eastward shift of El Niño teleconnections over the U.S. (Fig. 1d), the
194 future pattern of frost days during El Niño events (Fig. 2c) shows the anomalous decrease
195 of frost days expanding eastward as well, with decreases in frost days in future El Niño
196 events now occurring as far east as the central part of the country, with a concomitant
197 reduction in the increased frost days over the eastern seaboard.

198

199 Fig. 3a indicates that during observed El Niño events, there is anomalously intense winter
200 precipitation in the SW U.S., across the southern tier of states, and along the eastern

201 seaboard, with decreases of precipitation intensity in the Pacific Northwest and Midwest.
202 The model control simulation shows similar patterns of precipitation intensity with the
203 exception of the area of decreased precipitation intensity in the Midwest (Fig. 3b). For
204 future El Niño events, the area of anomalously intense precipitation in the southwest
205 expands eastward and northward to cover the entire west coast region, and areas of
206 increased precipitation intensity in the southeast U.S. become stronger (Fig. 3c).
207 Decreases of precipitation intensity become established in the Midwest. These changes
208 in the pattern of precipitation intensity change for future El Niño events can again be
209 traced to the change in teleconnection pattern, with a northward and eastward shift of the
210 anomalous low pressure in the north Pacific resulting in more intense precipitation along
211 the length of the west coast, and the deepening of low pressure in the Atlantic producing
212 more intense precipitation along the eastern seaboard in future events.

213

214 During present-day El Niño events, observations show decreases of heat wave intensity
215 over much of the southern tier of states, with increases in the upper Great Plains and
216 southern Rockies (Fig. 4a). A similar but stronger pattern is evident in the model control
217 run (Fig. 4b). For future El Niño events, there is a marked change in the pattern, with the
218 decreases of heat waves in the southern tier turning to increases (Fig. 4c) that is
219 associated with the change of the teleconnection.

220

221 **5. Conclusions**

222

223 A global coupled climate model (PCM), analyzed in previous studies of changes of
224 extremes, is used here to illustrate possible changes of patterns of extremes during El
225 Niño events over the continental U.S. in a future warmer climate. The model is able to
226 simulate most first order aspects of teleconnection patterns of winter SLP over the U.S.
227 for present-day El Niño events, with a notable systematic shift of the pattern southward
228 and eastward with consequent shifts of the patterns of extremes during El Niño events.
229 The patterns of frost days, precipitation intensity and heat waves are compared to
230 observations to show that the model is able to simulate most of the main features of
231 present-day extremes associated with El Niño events. Previous studies have shown the
232 changes in the pattern of teleconnections over the U.S. for the end of the 21st century are
233 mostly due to changes in the midlatitude base state circulation due to the increase of
234 GHGs in the atmosphere. This change in teleconnections produces changes in the
235 patterns of extreme events associated with future El Niño events such that anomalous
236 decreases of frost days expand eastward, anomalously intense precipitation in the SW
237 U.S. expands eastward with areas in the SE U.S. becoming stronger, and decreases of
238 heat wave intensity in the control run over much of the southern tier of states turn to
239 increases during future El Niño events.

240

241

242

243

244

245

246 **Acknowledgements**

247

248 Portions of this study were supported by the Office of Science (BER), U.S. Department
249 of Energy, Cooperative Agreement No. DE-FC02-97ER62402, and the National Science
250 Foundation. The National Center for Atmospheric Science is sponsored by the National
251 Science Foundation. We thank Servicio Meteorológico Nacional of the Comisión
252 Nacional del Agua and Environment Canada for providing the Mexican and Canadian
253 daily data used in this analysis.

254

255

256

257

258

259

260

261

262

263

264

265

266

267

268

269 **References**

270

271 Alexander, L.V., and co-authors (2006), Global observed changes in daily climate
272 extremes of temperature and precipitation. *J. Geophys. Res.*, *111*, D05109,
273 doi:10.1029/2005JD006290.

274

275 Cayan, D.R., K.T. Redmond, and L.G. Riddle (1999), ENSO and hydrological extremes
276 in the western United States. *J. Climate*, *12*, 2881—2893.

277

278 Easterling, D. R., and co-authors (2000), Climate extremes: Observations, modeling and
279 impacts. *Science*, *289*, 2068–2074.

280

281 Frich, P., L.V. Alexander, P. Della-Marta, B. Gleason, M. Haylock, A.M.G. Klein Tank,
282 and T. Peterson (2002), Observed coherent changes in climatic extremes during the
283 second half of the twentieth century. *Clim. Res.*, *19*, 193--212.

284

285 Gershunov, A., and T.P. Barnett (1998), ENSO influence on intraseasonal extreme
286 rainfall and temperature frequencies in the contiguous United States: Observations and
287 model results. *J. Climate*, *11*, 1575—1586.

288

289 Glantz, M.H. (2001), *Currents of Change: El Niño and La Niña Impacts on Climate and*
290 *Society*. Second edition, Cambridge, UK: Cambridge University Press. 252 pp.

291

292 Karl, T.R., and R.W. Knight (1997), The 1995 Chicago heat wave: How likely is a
293 recurrence? *Bull. Amer. Meteorol. Soc.*, 78, 1107—1119.

294

295 Meehl, G. A., 1987: The annual cycle and interannual variability in the tropical Pacific
296 and Indian Ocean regions. *Monthly Weather Review*, **115**, 27–50.

297

298 Meehl, G. A., and co-authors (2000), An introduction to trends in extreme weather and
299 climate events: Observations, socio-economic impacts, terrestrial ecological impacts, and
300 model projections. *Bulletin of the American Meteorological Society*, 81, 413–416.

301

302 Meehl, G.A., and C. Tebaldi (2004), More intense, more frequent and longer lasting heat
303 waves in the 21st century. *Science*, 305, 994--997.

304

305 Meehl, G.A., C. Tebaldi, and D. Nychka (2004a), Changes in frost days in simulations of
306 21st century climate. *Clim. Dyn.*, 23, 495--511.

307

308 Meehl, G. A., W. M. Washington, C. Amman, J. M. Arblaster, T. M. L. Wigley, and C.
309 Tebaldi (2004b), Combinations of natural and anthropogenic forcings and 20th century
310 climate. *Journal of Climate*, 17, 3721–3727.

311

312 Meehl, G. A., J. M. Arblaster, and C. Tebaldi (2005a), Understanding future patterns of
313 precipitation extremes in climate model simulations. *Geophysical Research Letters*, 32,
314 No. 18, L18719, doi: 10.1029/2005GL023680.

315

316 Meehl, G.A., W.M. Washington, W.D. Collins, J.M. Arblaster, A. Hu, L.E. Buja, W.G.
317 Strand, and H. Teng (2005b), How much more global warming and sea level rise?
318 *Science*, 307, 1769--1772.

319

320 Meehl, G. A., H. Teng, and G. W. Branstator (2006), Future changes of El Niño in two
321 global coupled climate models. *Climate Dynamics*, doi: 10.1007/s00382-005-0098-0.

322

323

324 Meehl, G.A., and H. Teng (2007), Multi-model changes in El Niño teleconnections over
325 North America in a warmer climate. *Cli. Dyn.*, in press.

326

327 Meehl, G. A. and coauthors (2007a), Global Climate Projections, In: *Climate Change*
328 *2007: The Scientific Basis*. Contribution of Working Group I to the Fourth Assessment
329 Report of the Intergovernmental Panel on Climate Change, S. Solomon, Q. Dahe, and M.
330 Manning, Eds., Cambridge University Press, in press.

331

332 Meehl, G. A., C. Covey, T. Delworth, M. Latif, B. McAvaney, J. F. B. Mitchell, R. J.
333 Stouffer, and K. E. Taylor (2007b), The WCRP CMIP3 multi-model dataset: A new era
334 in climate change research, *Bulletin of the American Meteorological Society*, in press.

335

336 Meehl, G.A., J.M. Arblaster and C. Tebaldi (2007c), Contributions of natural and
337 anthropogenic forcing to changes in temperature extremes over the U.S.

338 *Geophys. Res. Lett.*, submitted.

339

340 Peterson, T.C., X. Zhang, M. Brunet, J.L. Vázquez (2007) Changes in North American
341 extremes derived from daily weather data. *Proceedings of the National Academy of*
342 *Science*, submitted.

343

344 Schubert, S.D., Y. Chang, M. Suarez, and P. Pegion (2005), On the relationship between
345 ENSO and extreme weather events over the contiguous United States. U.S. CLIVAR
346 Variations, V3N3.

347

348 Tebaldi, C., J.M. Arblaster, K. Hayhoe, and G.A. Meehl (2006), Going to the extremes:
349 An intercomparison of model-simulated historical and future changes in extreme events.
350 *Clim. Change*, 79, doi 10.1007/s10584-006-9051-4.

351

352

353

354

355

356

357

358

359

360

361

362

363 **Figure captions**

364

365 Fig. 1: upper left: composite SLP anomalies (DJF), El Niño minus La Niña, for the
366 model control run events; middle left: same as (upper left) except for observations;
367 lower left: differences, model minus observations, of El Niño teleconnection patterns;
368 upper right: same as (upper left) except for the stabilized A1B future climate experiment;
369 middle right: differences, future minus control, for model-simulated El Niño event
370 teleconnections (all in Pa).

371

372 Fig. 2: a) composites of observed frost days, El Niño events minus La Niña events
373 (days); b) same as (a) except for the model control run; c) same as (b) except for the
374 stabilized A1B future climate experiment.

375

376 Fig. 3: same as Fig. 2 except for precipitation intensity (mm day^{-1}).

377

378 Fig. 4: same as Fig. 2 except for heat wave intensity ($^{\circ}\text{C}$).

379

380

381

382

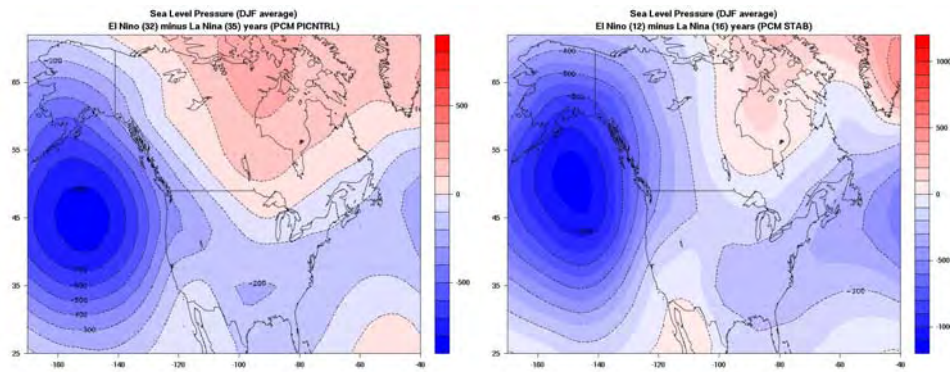
383

384

385

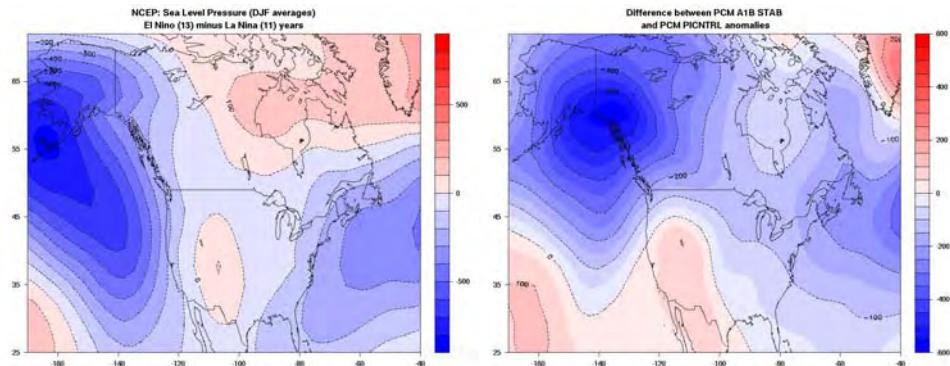
386

387

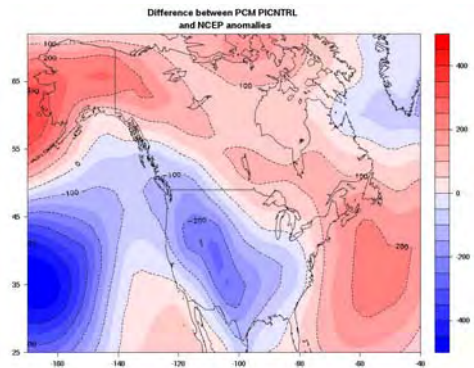


388

389



390



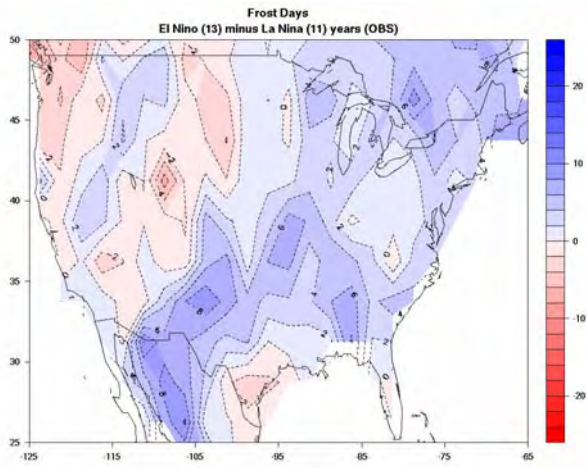
391

392

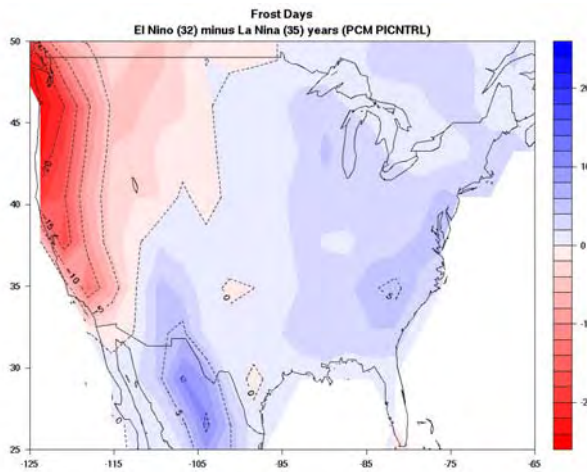
393

394 Figure 1

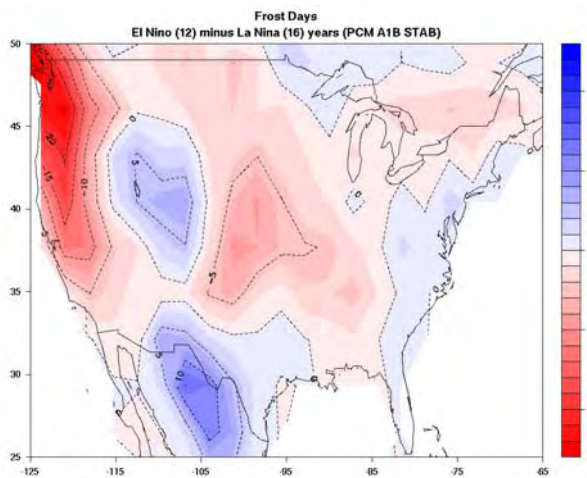
395



396



397

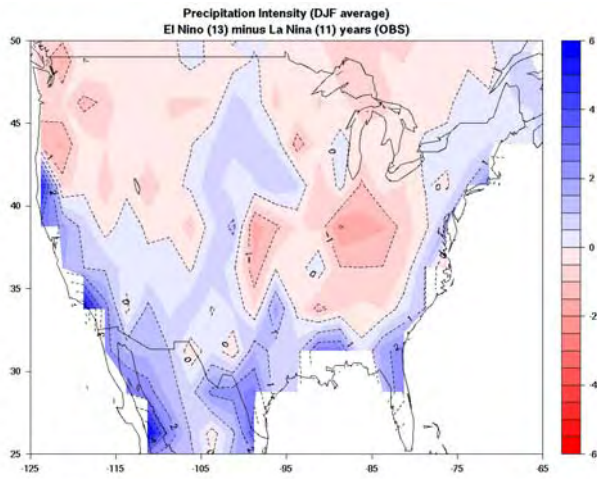


398

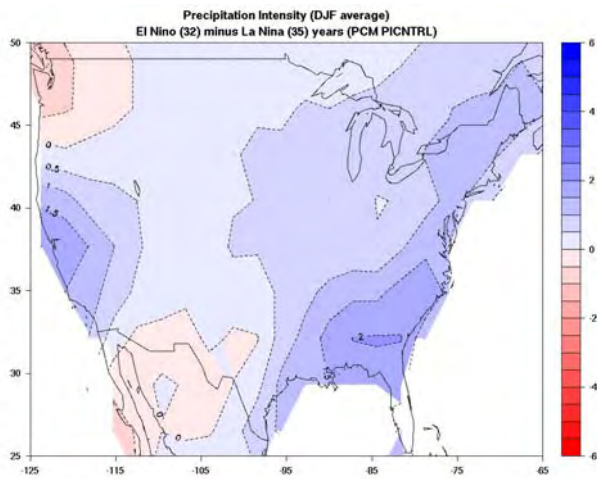
399

Figure 2

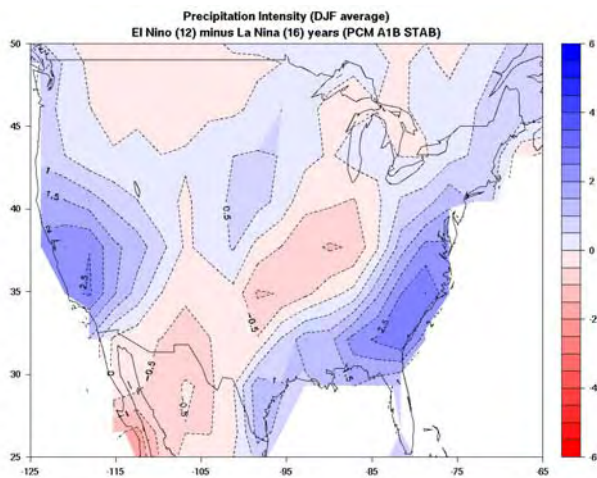
400



401



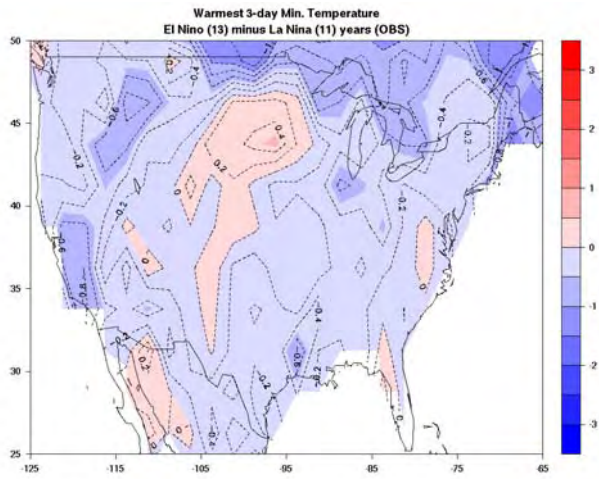
402



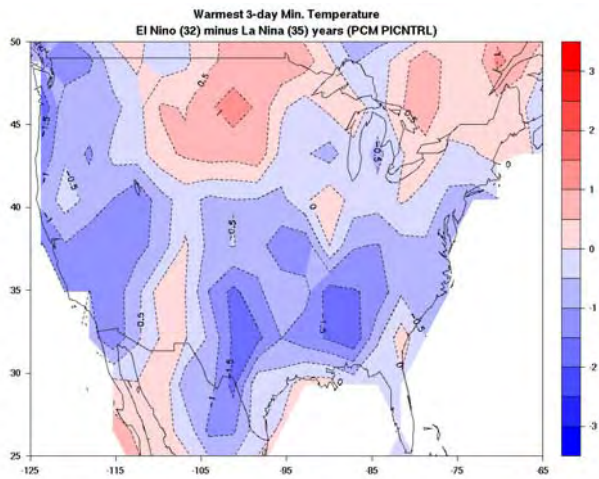
403

404 Figure 3

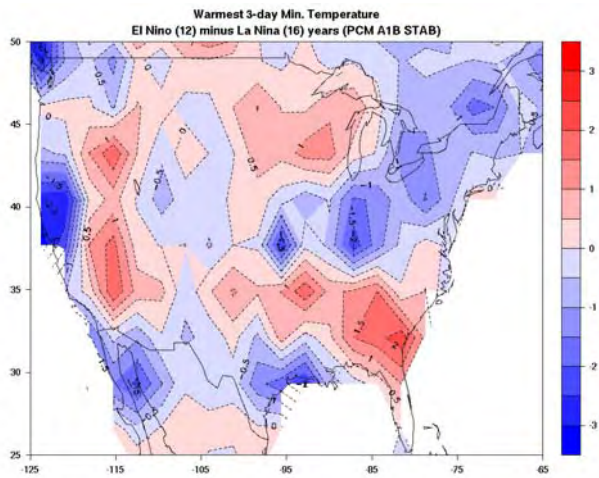
405



406



407



408

409 Figure 4

